CONFORMATIONAL KINETICS OF TRILIGATED HEMOGLOBIN

FRANK A. FERRONE, ANTHONY J. MARTINO, AND SOUMEN BASAK
Department of Physics and Atmospheric Science, Drexel University, Philadelphia, Pennsylvania 19104

ABSTRACT We have used the method of modulated excitation (Ferrone, F. A., and J. J. Hopfield, 1976, *Proc. Natl. Acad. Sci. USA.* 73:4497–4501), with an improved apparatus and a revised analytical procedure, to measure the rate of conformational change between the oxy (R) and deoxy (T) conformations of triligated carboxy-hemoglobin A at pH 6.5 and 7.0. We have found the rates to be $k_{RT} = 1.2 \times 10^3\ s^{-1}$ and $k_{TR} = 3.5 \times 10^3\ s^{-1}$ for pH 6.5, while for pH 7.0, $k_{RT} = 1.0 \times 10^3\ s^{-1}$, and $k_{TR} = 3.0 \times 10^3\ s^{-1}$. The value for L_3, the equilibrium constant between conformations, was virtually unchanged between pH 6.5 and 7.0. While the rates measured here differ from those obtained in the original use of this method, these new rates are fully consistent with the original data when analyzed by the revised procedures presented here. When taken with other kinetic and equilibrium data, our measurements suggest that the transition state between structures is dominated by the behavior of the T quaternary structure. Finally, a spectral feature near the HbCO Soret peak has been observed that we ascribe to an allosteric perturbation of the spectra of the liganded hemes.

INTRODUCTION

Proteins are increasingly recognized as dynamic engines rather than static structures, and the fluctuations that proteins undergo have come under broad investigation (1–4). An important component of such investigations is the study of how conformational change is regulated by a protein. Hemoglobin's extensively studied quaternary structure change provides a useful model for such work. The two alternative quaternary structures are known in atomic detail (5), the thermodynamics of the transition is generally understood (6–10), and model calculations of the structural relaxation have already been initiated (11, 12).

The first measurement of the rate of hemoglobin's quaternary structure change was performed by photolysis experiments using an intense flash of light to produce a deoxy species, originally called a quickly reacting Hb or Hb* (13), and subsequently identified with the zero-liganded, oxy quaternary structure, i.e., R_0 (10). Sawicki and Gibson extended those photolysis experiments by using a laser as a photolysis source, and began the first systematic study of the variation of the allosteric rates (14, 15). By using partially oxidized samples, Cho and Hopfield employed a similar photolysis technique to measure the rate of conformational change of the singly liganded oxy species, R_1 (16). Most recently, Hofrichter et al. have followed the conformational change kinetically and spectroscopically from time as short as nanoseconds (17). All of the above measurements, however, follow the transition as the molecule switches from R to T.

The method of modulated excitation provided a new way to measure the rate of quaternary relaxation of hemoglobin (18). The intense laser photolysis pulse was replaced by a weak, periodic photolytic excitation so that at most one ligand per tetramer is removed. The use of periodic excitation allowed the spectrum of the excited species to be observed by scanning a monochromator, as well as providing for signal averaging to reduce noise. While these advantages are equally applicable to repetitively pulsed excitation, the unique approach of the modulation method is to employ phase tuning to reveal in real time the spectra of smaller relaxation components. Thus, in practice, a given modulation frequency is selected, a wavelength dominated by a given relaxation component is chosen, and the phase of the detection system is tuned to maximize the reponse. Flipping the phase by 90° then presents a data channel from which the given relaxation has been removed by this phase tuning procedure. Any other relaxation with a different spectrum and a different phase (i.e., different relaxation rates) can then be observed in this 90° channel. Rates are then determined by collecting such phase-tuned spectra at many frequencies, and following the magnitude of the spectra observed. For the method to be most effective, the spectra of the species investigated should be known a priori, although there do exist procedures for discovering the spectra without such knowledge.

The value of the method was not only that a new rate of structure change could be obtained, but that rate pairs naturally resulted. This directly gives the free energy difference between the conformations involved in the transition. Hence, as conditions are varied, it is possible to distinguish effects on the rates due to the alteration of the equilibrium constant for the final states from effects due to alteration of the transition state. In this way, it becomes possible to study those features that govern the rate of transition between conformations of hemoglobin.

In an earlier communication, the essentials of the method were outlined, and its application to the measurement of the rate of conformational change illustrated (18). In this paper we give a full development of the method, along with criteria to judge its applicability. (In the Appendix we give a quantitative criterion to be used in determining when excitations are appropriately small.) We find that some of the approximations used in the previous analysis break down, and must be replaced by revised procedures, which we describe as well.

Using an improved apparatus and the revised procedures, we have measured relaxation rates for the quaternary structure change R $\rightarrow$ T as well as T $\rightarrow$ R for triligated carboxy-HbA at pH 6.5 and 7.0. From this data we obtain the relative populations of molecules in the oxy and deoxy quaternary structures with three ligands bound, i.e., we directly determine the allosteric equilibrium constant L_3. The new rates differ significantly from those found previously (18), but when coupled with the revised analysis provide a complete and consistent explanation of the previous data. When taken with other kinetic and equilibrium data available, our measurements suggest that the transition state between structures is dominated by the behavior of the deoxy or T quaternary structure. We have also identified a spectral feature that we ascribe to an allosteric perturbation of the CO spectrum.

THEORY

Although the basic theory of modulated excitation has been described previously (18) we give a complete exposition here to facilitate discussion of the necessary modifications. We use an allosteric model modified to describe kinetics as developed by Hopfield et al. (19) in which the hemoglobin tetramer is viewed as having only two significant quaternary structures, R and T, and five possible states of ligation. We shall designate the population of a given quaternary state as R_j or T_j where j stands for the number of ligands bound. We assume that these thermodynamic states correspond to actual structural species. The rate of change of the population R_3 is given by

$$dR_3/dt = (dR_4/dt)_{photo} - (dR_3/dt)_{photo} + k_4'R_4 - k_3R_3 + k_{TR}T_3 - k_{RT}R_3 - k_3'R_3 + k_2R_2, \quad (1)$$

where $(dR_j/dt)_{photo}$ represents the rate of photolysis from the j-liganded species, k_j' represents the spontaneous ligand release rate, k_j represents the ligand binding rate, and k_{TR} and k_{RT} represent the rate of crossing from T to R and vice versa. The equation for dT_3/dt will look the same, except for appropriate index changes of R to T and vice versa. For CO, we can neglect the off rates, k_j'; for binding to the R state, $k_3 = k_R$, and $k_2 = 2k_R$. In the equation for the T_3 state, of course, $k_3 = k_T$ and $k_2 = 2k_T$. To simplify the appearance of the equations we are not explicitly writing the [CO] dependence of the binding rates k_R and k_T. The rate of photoexcitation is proportional to the absorbed photon intensity, I_{abs}, and the latter can be related to the extinction coefficient, ϵ, path length, l, and concentration of absorbing species. Thus

$$(dR_j/dt)_{photo} = Q_R I_{abs} = Q_R I_{in}[1 - \exp(-2.3\,\epsilon\, l R_j)] \quad (2a)$$

$$= Q_R I_{in}\, 2.3\,\epsilon\, l R_j, \quad (2b)$$

where the last step assumes that R_j is small. Here Q_R is the quantum efficiency for the R state. The incoming flux of light, I_{in}, is modulated at frequency ω, and can be written in terms of the average intensity $\langle I \rangle$ as

$$I_{in} = \langle I \rangle [1 + e^{i\omega t}], \quad (3)$$

where we have used imaginary numbers to simplify discussions below (and $i = \sqrt{-1}$). The presence of the 1 in the bracketed sum keeps the intensity positive. Thus the excitation rate is

$$(dR_j/dt)_{photo} = A_{Rj}R_j[1 + e^{i\omega t}], \quad (4)$$

where A_{Rj} contains all the proportionality factors. For any species, R_j, the response to the sinusoidal perturbation may have harmonic terms of ω and higher multiples, as well as a DC term. Thus we can put

$$R_j = \sum_{n=0} R_{j,n}\, e^{in\omega t}. \quad (5)$$

By substituting this into Eq. 1 we get a set of equations that can be separated according to their orders of ω. Thus the first order terms of Eq. 1 are

$$i\omega R_{3,1} = A_{R4}R_{4,1} + A_{R4}R_{4,0} - A_{R3}R_{3,1} - A_{R4}R_{3,0} - k_R R_{3,1} + k_{TR}T_{3,1} - k_{RT}R_{3,1} + 2k_R R_{2,1}. \quad (6)$$

If we take the small excitation limit, we assume $R_{4,0} \gg R_{4,1} \gg R_{3,1} \gg R_{2,1}$. (In the Appendix we discuss the conditions needed for the small excitation limit to be valid.) Eq. 6 reduces to

$$i\omega R_{3,1} = A_{R4}R_{4,0} - A_{R3}R_{3,1} - k_R R_{3,1} + k_{TR}T_{3,1} - k_{RT}R_{3,1} \quad (7)$$

and likewise we get

$$i\omega T_{3,1} = A_{T4}T_{4,0} - A_{T3}T_{3,1} - k_T T_{3,1} + k_{RT}R_{3,1} - k_{TR}T_{3,1}. \quad (8)$$

If we further assume that $T_{4,0} \ll R_{4,0}$, and that all the A's are small, we have essentially the equations of Ferrone and Hopfield (18)

$$i\omega R_{3,1} = A_{R4}R_{4,0} - k_R R_{3,1} + k_{TR}T_{3,1} - k_{RT}R_{3,1} \quad (9a)$$

$$i\omega T_{3,1} = -k_T T_{3,1} + k_{RT}R_{3,1} - k_{TR}T_{3,1}. \quad (9b)$$

If the small excitation limit has been reached so that we can use Eqs. 9, then we need to consider how these populations are measured. The detection system records a signal V, which is the result of a given population and a specific spectral weight. The spectral weight will depend on the monitoring wavelength, λ, while the population will only depend on the excitation frequency ω. Thus

$$V(\omega, \lambda) = s_R(\lambda)R(\omega) + s_T(\lambda)T(\omega) \quad (10a)$$

$$= s_R(\lambda)[R(\omega) + T(\omega)] + s_{TR}(\lambda)T(\omega), \quad (10b)$$

where s_R is the difference spectrum for excitation to the R state, s_T is the difference spectrum for excitation to the T state, and $s_{TR} = s_T - s_R$, i.e., the difference spectrum between the deoxy R and T states. We have temporarily dropped the subscripts for the R and T states because, in the limit of small excitation, we only have R_3 and T_3 states to consider. However, Eq. 10 is totally general if we write

$$R(n\omega) = \sum_{j=0}^{4} (4 - j)R_{j,n} \quad (11)$$

and similarly for T, where the factor $(4 - j)$ appears so as to count deoxy hemes (i.e., the doubly-deoxy species will contribute twice as much to the spectra). Suppressing the ω labels, Eq. 10 can be written as

$$V = (R + T)\{s_R(\lambda) + s_{TR}(\lambda)\,[T/(R + T)]\}. \quad (12)$$

The quantity V is a complex number, whose real and imaginary parts represent, respectively, the detected signal in phase and out of phase with

the excitation. The lock-in amplifier detection system can be phase tuned, which is equivalent to multiplying V by $\exp(i\phi_0)$ where ϕ_0 is the phase angle by which the lock-in tuning has been changed. Tuning (selection of ϕ_0) is done as follows: We go to a wavelength λ^* where $s_{TR}(\lambda^*) = 0$ (i.e., an isosbestic of the TR difference spectrum). At this wavelength all the phase information in V arises from the R + T signal. We then adjust the lock in phase, ϕ_0, so that V is entirely real, i.e., V is in the in-phase channel, and the out-of-phase channel is zero. (If the R + T signal is written as $|R + T|\exp(i\phi)$ then we have adjusted the detector phase so that $\phi_0 = -\phi$.) If we call this newly tuned signal V', the imaginary part is solely contributed by the crossing kinetics between R and T. That is,

$$\mathrm{Im}V' = |R + T|\, s_{TR}(\lambda)\mathrm{Im}[T/(R + T)]. \quad (13)$$

Once the tuning is accomplished for a given frequency ω, the wavelength is swept, providing the entire spectrum s_R or s_{TR}. For the out-of-phase channel, the coefficient of the spectrum is just $|R + T|\mathrm{Im}[T/(R + T)]$; for the in-phase channel, the signal is Re V', and the coefficient of the $s_R(\lambda)$ spectrum is $|R + T|$. Hence, if we measure the out-of-phase spectrum and determine the coefficient of $s_{TR}(\lambda)$ and divide it by the coefficient of the spectrum $s_R(\lambda)$ from the in-phase channel, we obtain $\mathrm{Im}[T/(R + T)]$. By using Eq. 9b, we see that this latter quantity is related to the kinetics of the conformational change, namely,

$$\mathrm{Im}[T/(R + T)] = -\omega k_{RT}/\{(k_{RT} + k_{TR} + k_T)^2 + \omega^2\}. \quad (14)$$

This equation can be readily written in a linear form in ω^2, namely,

$$(1/k_{RT})\omega^2 + (k_{RT} + k_{TR} + k_T)^2/k_{RT} = -\omega/\mathrm{Im}[T/(R + T)]. \quad (15)$$

Thus if we plot $-\omega/\mathrm{Im}[T/(R + T)]$ as a function of ω^2, the slope of such a linearized plot is the reciprocal of k_{RT} and the intercept on the ω^2 axis is the quantity $(k_{RT} + k_{TR} + k_T)^2$.

Several points in Eq. 15 are worth noting. With the exception of k_T, which is normally quite small, the ligand binding process has been tuned out by this procedure, and its kinetics do not appear. Although the difference spectra must be known to obtain their coefficients by curvefitting, some information is still obtained if only the shape (and not the scale) is known. The x-intercept in Eq. 15 will not depend on the y-scale, so that the sum of all the rates is obtained even for uncalibrated spectral data.

For following the ligand binding signal, the tangent of ϕ, the absolute phase of the total detected signal, is employed. This is defined as

$$\tan\phi(\omega, \lambda) = \mathrm{Im}V(\omega, \lambda)/\mathrm{Re}V(\omega, \lambda); \quad (16)$$

that is, the out of phase over the in-phase signal. If we follow the tangent at an isosbestic of the RT transition, s_{TR} is zero, and we have

$$\tan\phi = \mathrm{Im}(R + T)/\mathrm{Re}(R + T). \quad (17)$$

In the limit in which k_{RT} and k_{TR} are much greater than k_R or k_T, we find that $\tan\phi = -\omega/k_R$. This equation also results when ω becomes larger than the various rates. In general, however, the limit giving this simple behavior is not achieved even when the small excitation limit is reached. Thus a full solution of Eq. 9 (small excitation) or Eq. 6 must be employed in calculating R + T for Eq. 17.

Although the theory described here is similar to that of Ferrone and Hopfield (18), a number of important differences should be noted. First, the previous treatment did not include the 1 in Eq. 3. Addition of this term leads to a number of cross-terms which, although unimportant in the small excitation limit, do matter when higher excitation is considered. Second, the earlier development included only the imaginary part of T/R, rather than the imaginary part of T/(R + T). Although the magnitude of T is expected to be smaller than R, this correction introduces an important phase relationship. This is why, in the analysis of the previous data, the ω^2 intercept was given only as k_{TR}^2, rather than the sum seen in, e.g., Eq. 15. Third, the small excitation limit does not arise as readily as once expected, with the result that the full form of Eq. 6 must be used. While this does produce a soluble set of linear equations, those equations are clearly more cumbersome than the simple treatment outlined above. (The Appendix provides quantitative criteria for determining when the small excitation limit can be used.) Finally, the expression for the tangent of phase (Eq. 17) does not assume simple linearity in frequency as readily as previously assumed.

EXPERIMENTAL METHODS

Hemoglobin was obtained from the Red Cross (Philadelphia, PA) and prepared from pooled blood according to standard methods (19, 20). After passage through a column of cellulose (DE52; Whatman Inc., Clifton, NJ) one quarter of the central pooled fractions was saved by quick freezing drops in liquid nitrogen. Hemoglobin was stored frozen until use. For use, one or more frozen droplets were thawed and dialyzed against 0.15 M phosphate buffer, at pH 6.5 or 7.0. The hemoglobin was then placed into 1 ml vials, and flushed with water-saturated CO.

The preparation of a sample for investigation was done in a glove box, through which water-saturated carbon monoxide was flowed. Samples were prepared by placing 2–5 μl onto a 24 by 50 mm coverslip, covered by a 22 × 22 mm coverslip, and sealed into place by dental wax. A thin layer of petroleum jelly acted as a spacer for the upper coverslip. The sample thickness was controlled to give a peak absorbance in the Soret band of ~1; the sample was used at once. Sample concentration was 1 mM heme, as measured on an aliquot taken from the vial, using the cyanomet derivative. Concentrated dithionite solution was added to give a final dithionite concentration of 2 mM.

The excitation/photolysis source was the 514 nm line of an argon ion laser (Spectra-Physics Inc., Mountain View, CA). Power at the laser head varied from 200–600 mW, and was attenuated by subsequent reflection losses, and in some cases by neutral density filters. The laser was incident on the sample at 45° and focused to a spot with a Gaussian diameter of ~2 mm. Thus power at the sample was always $\lesssim$4 W/cm^2. (For comparison, note that 100% photolysis on this sample would require ~100 W/cm^2 [22].) Modulation was provided by an Isomet acousto-optic modulator, with frequency set by a frequency generator (model 182A; Wavetek, San Diego, CA). Frequency was measured by a Hewlett-Packard model 5314A frequency counter (Hewlett-Packard Co., Palo Alto, CA), accurate to 0.1 Hz. The sample was clipped to a Cambion thermoelectric stage, set to 19.0°C.

The probe beam for the system was provided by a 150 W xenon arc lamp, passed through an Oriel f/3.7 grating monochromator, with slits set for 3.2 nm resolution. The optical configuration is that of a horizontal microspectrophotometer assembled on an NRC optical table, and employing long working distance 10× objectives (E. Leitz, Inc., Rockleigh, NJ). The probe beam was masked to occupy a region on the sample 1 mm square in the center of the laser spot. The signal was detected by a photomultiplier with a shortened dynode chain (9798B; EM Industries, Inc., Cherry Hill, NJ), and a similar phototube was used as a reference when taking absorbance spectra. A set of filters blocked scattered laser light from the phototubes.

The AC signal is processed by a two-phase lock-in amplifier (Ortec 9505, EG & G Instruments, Princeton, NJ) operated in SC mode to suppress harmonic response. The DC part of the signal from the photomultiplier, as well as the DC outputs from the lock-in are digitized (12 bits) and processed by an LSI 11/03 computer. The difference spectrum from the detection system is computed by using the LSI 11 to divide out the DC intensity, rather than by using dynode feedback. The system allows an absorbance spectrum, as well as in-phase and out-of-phase difference spectra to be collected simultaneously. The out-of-phase spectrum was typically recorded with a 10-fold greater gain, produced by the lock-in amplifier post-mixer amplification stage. The computer controls the monochromator by advancing a stepping motor, so that during data collection a minimum of vibrations are present, and data gathering may proceed for as long as desired, with the computer averaging the incoming signal. Data is stored on disk for later analysis.

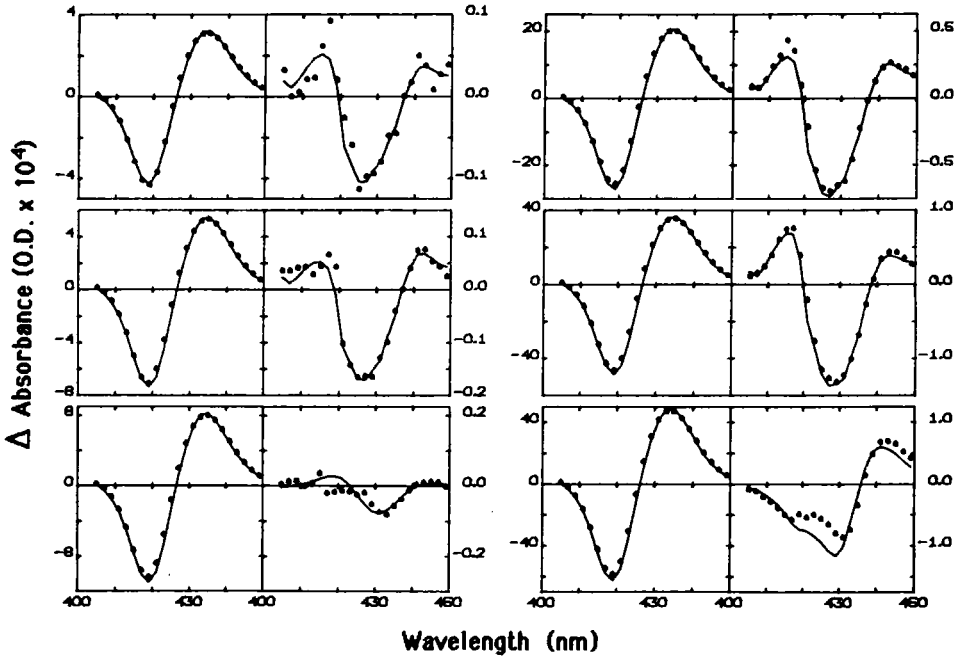

FIGURE 1 Typical modulated spectra. Spectra are shown in pairs; the *left hand* member is the spectrum in the in-phase channel, while the *right hand* member is the out-of-phase channel. The data shown is for one pH 6.5 experiment. The six *left hand* figures were taken with the lowest laser power (67 mW at the laser head) while the *right hand* panels were taken with the highest power (600 mW at the laser head). Experiments are shown for three modulation frequencies: 1,004.4 Hz, 498.8 Hz, and 99.8 Hz (from *top* to *bottom*). The solid curves are the best fits to the data of three spectra: the CO-deoxy difference spectrum, the R–T difference spectrum, and the synthesized spectrum described in the text. Note that the CO-deoxy spectrum dominates the in-phase channel, while the R–T difference spectrum dominates the out-of-phase channel.

In obtaining modulated spectra small synchronous signals were observed in both channels, due to electronic pickup and small amounts of scattered laser light (never more than ~0.3% of full scale). Prior to taking a spectrum, these signals were nulled on the lock-in amplifier. For measurements of tan ϕ it is necessary to obtain an absolute phase. This was done by blocking the monochromator, and removing the laser filters and then tuning to the laser scattered light.

Recorded spectra were analyzed by error-weighted linear curvefitting to standard spectra. Absorption standards for HbCO and deoxyHb were obtained using a Cary 17 spectrophotometer in the Laboratory of Chemical Physics, at the National Institutes of Health (F. Ferrone, unpublished results). The difference spectrum for the allosteric change was obtained by digitizing the spectrum obtained upon the addition of inositol hexaphosphate to NES-des Arg Hb (23). By a number of different methods, this modified hemoglobin has been shown to switch its structure upon the addition of IHP (23). The results are not strongly sensitive to the choice of this modified hemoglobin for an allosteric standard spectrum, as explained in the Discussion.

The coefficients of the modulated spectra give the populations in and out of phase relative to ligand binding. Those coeffieicients were analyzed as described in the Theory section. Nonlinear curvefitting was carried out on the Drexel University PRIME computer using the routine of Bevington (24).

RESULTS

Modulated spectra from 400–450 nm were collected at frequencies of 100, 250, 500, 700, and 1,000 Hz. At each frequency, spectra were collected at four different laser intensities, with the total intensity variation being roughly a factor of 10. The degree of photolysis achieved varied from ~0.1% of the sample to as much as 2% of the sample, as determined by fitting the in-phase spectrum to the standard COHb minus deoxyHb difference spectrum.

Each modulated spectrum was taken by tuning the phase of the lock-in detection system for a null at 436.5 nm, which is an isosbestic of the R–T difference spectrum. This

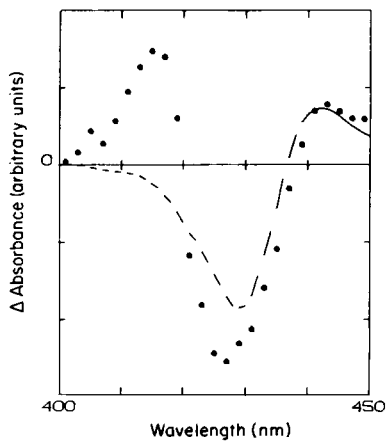

FIGURE 2 Construction of a synthesized spectrum. The points are the result of averaging seven spectra measured at 1 kHz. To set a mutual scale, each spectrum was normalized by it rms integrated area. The region from 438 to 450 nm was then fit by the R–T difference spectrum; the fit is shown as the solid curve. The dashed curve shows the remainder of the full R–T difference spectrum scaled by the fit coefficient. The synthesized spectrum was obtained as the difference between the experimental data and the dashed curve.

should make the ligand binding spectrum entirely dominant in one channel (the in-phase signal), and a projection of the spectrum of allosteric change dominant in the other channel (the out-of-phase channel) (18). Representative data is shown in Fig. 1. The signal observed in the out-of-phase channel is typically 40 times smaller than the in-phase signal. As can be seen, the noise level of the experiment is of the order of 10^{-6} OD. The worst signal-to-noise ratio occurs at the CO Soret peak, as the detected intensity drops by an order of magnitude. As frequency increases, the in-phase signal size begins to decrease, due primarily to the kinetics of the rebinding of CO. (Once $\omega > k_R[CO]$, the signal size decreases approximately as $1/\omega$.) On the other hand, the out-of-phase signal displays a broad maximum (see Eq. 14), and relative to the in-phase signal, varies much less in the frequency range studied.

The in-phase spectrum is well fit by the CO-deoxy difference spectrum plus the R–T difference spectrum. When the out-of-phase measured spectrum was fitted by a standard R–T difference spectrum (with or without a contribution from the CO-deoxy spectrum), a significant discrepancy was observed in the 400–425 nm region. Since the method of modulated excitation relies on correct assignment of the spectra of the various interconverting components, it is very important to identify all the constituent spectra. The spectral discrepancy seen could arise either because the spectrum of a known component is misconstrued, or because an unanticipated component was present contributing an unknown spectrum. The first problem would arise if, for example, the R–T difference spectrum measured in static experiments on modified hemoglobins were not equivalent to the kinetic R–T difference spectrum. We rejected this first alternative since the discrepancy in the out-of-phase spectrum changes as power and frequency are changed. If the spectrum of allosteric change were simply different, the same shape of spectrum should be seen at each power and frequency. We concluded that the failure of the curves to fit the data was due to the presence of an unexpected component.

To determine the shape of the spectrum causing the discrepancy, we employed the following procedure. First, an average spectrum was constructed from seven out-of-phase spectra taken at 1 kHz, as shown in Fig. 2. (In computing the average, each spectrum was weighted by the rms integrated area.) The long wavelength side resembles the expected R–T difference signal, whereas the low

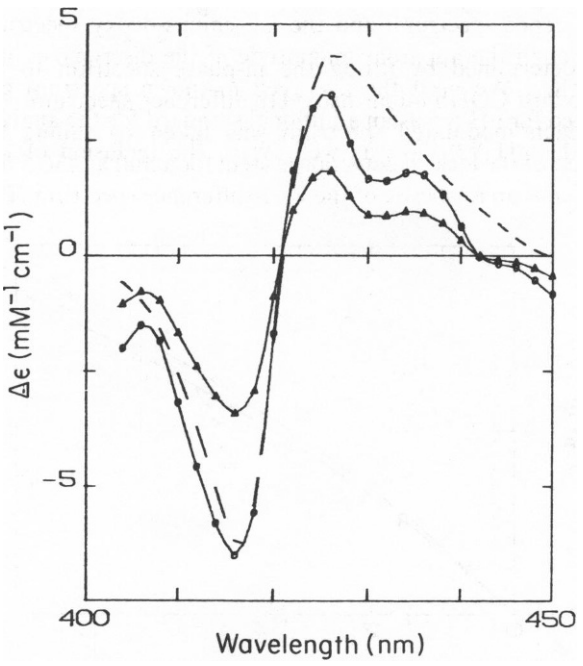

FIGURE 3 Synthesized difference spectrum. The subtracted spectrum obtained from the procedure described in the text and in Fig. 2 is shown as the data points, joined by a smooth curve as an aid to the eye. The same spectrum was used for both pH 6.5 and pH 7.0. Using the procedure described in the text, we set the scale for extinction coefficients as shown in the figure. Because the scale is different for each pH, two spectra are shown: The circles are the pH 6.5 spectrum, while the triangles are the pH 7.0 spectrum. The dashed curve is the difference spectrum seen upon addition of the allosteric effector IHP to Hb Trout IV with CO bound (34).

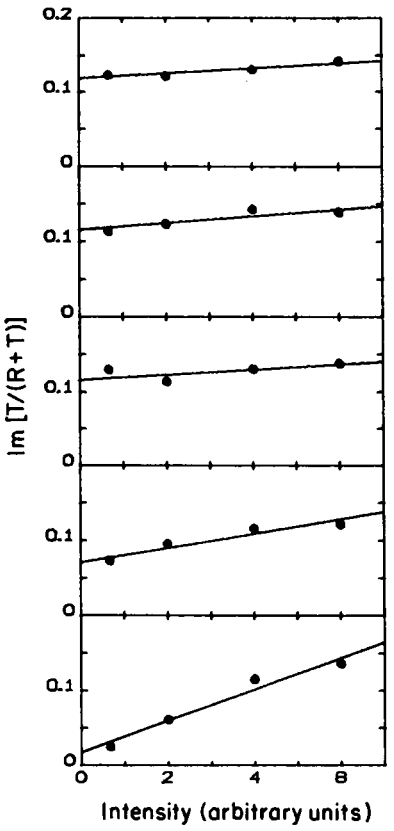

FIGURE 4 Typical zero power extrapolations. Data is shown for one experiment at pH 6.5. The y-axis is specified by dividing the coefficient of the R–T difference spectrum, determined from the out-of-phase spectrum, by the coefficient determined for the CO-deoxy difference spectrum. One unit on the x-axis represents 100 mw power at the laser head, or about 667 mw/cm^2 at the sample. All five frequencies are shown: (from *bottom* to *top*) 100 Hz, 250 Hz, 500 Hz, 700 Hz, and 1 kHz. The lines are the best fit straight lines; their y intercepts are used in subsequent analysis.

wavelength side differs considerably. We therefore assumed that the new contribution affected only the low wavelength region, and hence we subtracted out the standard spectrum R–T difference contribution. Specifically, the region from 438–450 nm was fit with the known R–T difference spectrum, to obtain a scale factor. The entire R–T difference spectrum was then scaled by this factor, and subtracted from the averaged spectrum. This yields a new difference spectrum, shown in Fig. 3. This new spectrum was in turn used as an additional standard with which to fit the in-phase and out-of-phase spectra as frequency and power were changed. The fits were noticably improved; fits are shown along with the data in Fig. 1.

For each frequency and power, the coefficient of the least squares fit of the R–T difference spectrum to the out-of-phase spectrum was divided by the coefficient for the CO-deoxy spectrum and the ratios of Im[T/(R + T)] were plotted as a function of laser intensity. A zero power intercept was constructed by linear extrapolation. Although the theory does not predict precise linearity, numerical simulations indicated that a linear approximation was reasonable, particularly in view of the scatter in the data obtained. A set of linear extrapolations for data at pH 6.5 is shown in Fig. 4.

The zero power intercepts were taken as the set of data for analysis as described for the small excitation limit in the Theory section. Linearized plots were constructed according to Eq. 15 for two separate experiments. As a means of averaging the data sets, we chose to plot the points on the same graph, rather than analyze the results of each experiment and then average the resultant rates. Fig. 5 shows this analysis for the pH 6.5 data. The reciprocal of the slope gives the R–T crossover rate at threefold ligation: it is found to be $1.2 \times 10^3\ s^{-1}$. The ω^2-intercept gives the square of the sum of the R → T, T → R rates, and the rate of CO binding in the T-state. If we take the latter value as $100\ s^{-1}$ (10, 27), we find that the T → R transition rate is $3.5 \times 10^3\ s^{-1}$. The ratio k_{RT}/k_{TR} gives a value of the allosteric constant, L_3, of 0.34. Though the points show some scatter, in general the linearity of the data is quite good.

Once these rates are determined, we could look at the overall kinetics as monitored by the frequency dependence of tan ϕ. We measured tan ϕ in absolute phase, as described above, for the lowest power excitation (67 mw at the laser head) for each of the five frequencies at which spectra were gathered. As shown in Fig. 6 the tangent is not perfectly linear in excitation frequency. Given the allosteric rates quoted above, however, the curvature is expected. (In control experiments on Mb a linear plot results.) The tan ϕ data was fit with a nonlinear least squares routine to determine $k_R[CO]$. Because the samples were prepared independently, it is possible that somewhat different CO saturation levels in the solution were achieved. Thus each tan ϕ curve was fit for $k_R[CO]$ separately. We find that the apparent ligand binding rates do vary, and are $4.3 \times 10^3\ s^{-1}$ and $4.6 \times 10^3\ s^{-1}$.

The analysis of the data collected at pH 7.0 proceeded in the same way. As observed for the pH 6.5 data, a discrepancy was found in the spectra when fit by the R–T difference spectrum, and the CO-minus-deoxy spectrum, although the apparent magnitude of the discrepancy was smaller. We used the averaged unknown spectrum collected for pH 6.5 as an additional standard for the analysis of the pH 7.0 data as well. With the inclusion of this

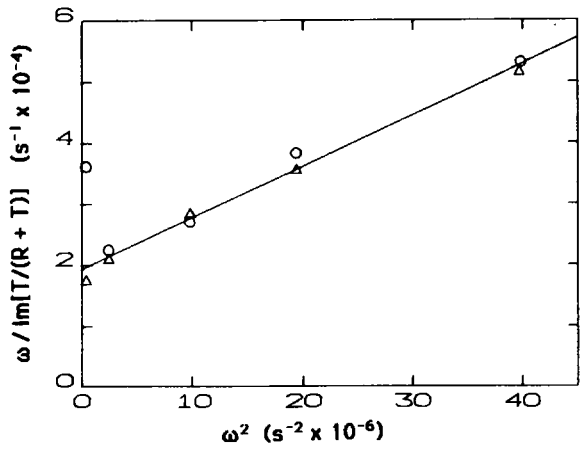

FIGURE 5 Analysis of the pH 6.5 R–T spectral coefficients according to the linearized form of Eq. 15. The y-values are obtained by multiplying the angular frequency, ω, by the reciprocal of the intercept in the zero-power extrapolation. The circles and triangles show two separate experiments at this pH. The straight line has been least-squares fit to the data; the reciprocal of the slope is k_{RT} and is found to be $1.2 \times 10^3\ s^{-1}$; the ω^2-intercept gives the sum $(k_{RT} + k_{TR} + k_T[CO])^2$, from which $k_{TR} = 3.5 \times 10^3\ s^{-1}$.

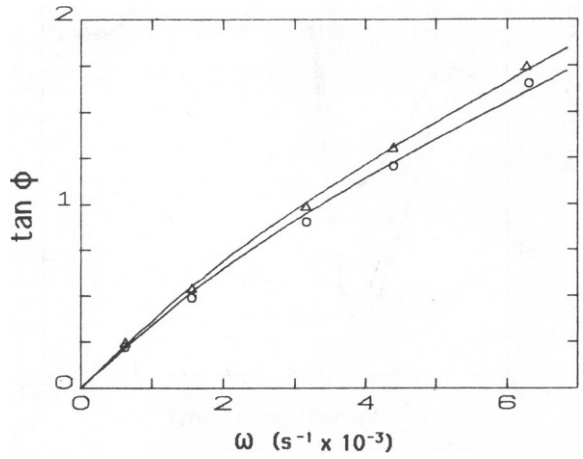

FIGURE 6 The frequency dependence of the tangent of absolute phase, for pH 6.5, measured at 436.5 nm. As described in the text, the ligand binding rate dominates the tangent, although the presence of curvature indicates that other effects (such as quaternary relaxation rates) are not absent. Using the quaternary relaxation rates measured here, the rate $k_R[CO]$ was determined by least squares fitting. Two experiments are shown, with slightly different apparent rates: $4.3 \times 10^3\ s^{-1}$ for the triangles, and $4.6 \times 10^3\ s^{-1}$ for the circles. As discussed in the text, the variation is likely due to different solution concentration of CO.

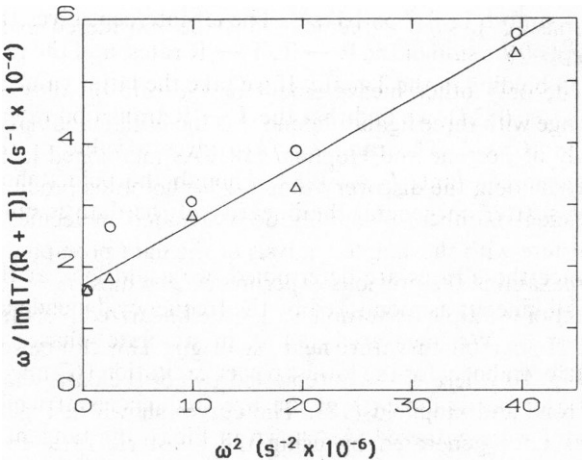

FIGURE 7 Analysis of the pH 7.0 R–T spectral coefficients according to the linearized form of Eq. 15. The procedure is exactly the same as for pH 6.5; again two experiments are shown. The slope determines k_{RT}, which is found to be $1.0 \times 10^3\ s^{-1}$; the ω^2-intercept then allows determination of k_{TR}, which is found to be $3.0 \times 10^3\ s^{-1}$.

spectrum, the agreement of the fits with the data became comparable to that seen for pH 6.5. Data collected at four incident laser intensities was used to extrapolate to a zero-power value, which was used in the linearized analysis described in Eq. 16. The linearized data plot obtained from this data is shown in Fig. 7. Again the data shows excellent linearity. We get an average R–T rate of $1.0 \times 10^3\ s^{-1}$ and an average T–R rate of $3.0 \times 10^3\ s^{-1}$. L_3 is 0.33 and virtually unchanged.

Fig. 8 shows the frequency dependence of the absolute tangent of phase for pH 7. Again there is noticeable curvature in the data, with greater variation between experiments than seen at pH 6.5. By nonlinear least-squares fitting, we find that the rate $k_R[CO]$ is $3.8 \times 10^3\ s^{-1}$ for one experiment, and $5.5 \times 10^3\ s^{-1}$ for the other. Note that, as expected, this variation does not affect the

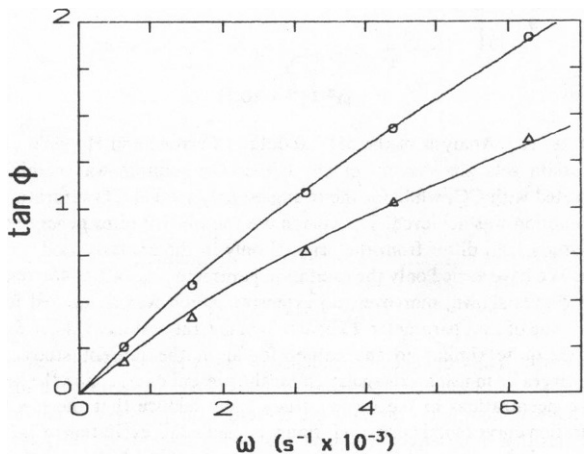

FIGURE 8 The frequency dependence of the tangent of absolute phase, for pH 7.0, measured at 436.5 nm. The procedure is exactly as for pH 7.0. Greater discrepancy is seen between the two experiments; for the circles, $k_R[CO] = 3.8 \times 10^3\ s^{-1}$, and for the triangles $k_R[CO] = 5.5 \times 10^3\ s^{-1}$.

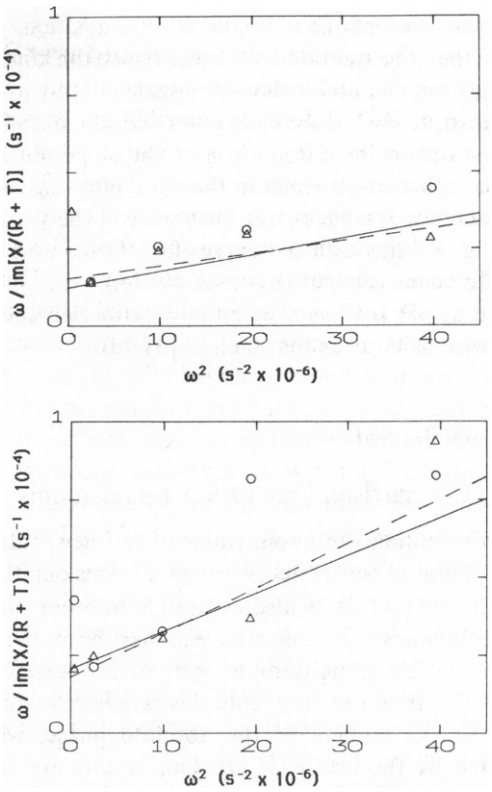

FIGURE 9 Analysis of the relaxation represented by the synthesized spectrum. Data is shown for both experiments for each of pH 6.5 (Fig. 9 *a*) and pH 7.0 (Fig. 9 *b*). The coefficient of the synthesized spectrum was used in a manner analogous to that employed for the coefficient of the R–T difference spectrum in extrapolating to zero power and constructing the linearized plots shown according to Eq. 15. Initially the *y*-axis is arbitrary because the extinction coefficient of the synthetic spectrum is unknown. The dashed curves show the unconstrained best straight line through the data. The solid line is the best fit, given that the ω^2-intercept for pH 6.5 and 7.0 is constrained to be the same as found in Figs. 5 and 7, respectively. By then requiring that the solid line have the same slope as in Fig. 5 or 7, the scale of the *y*-axis can be determined.

linearized plot. Reasons for this variation are discussed later.

Finally we turn to the coefficients of the unknown spectrum that arise in fitting the data. We processed these in the same way that we processed the coefficients of the R–T difference spectrum: for each pH, we extrapolated to zero power, and constructed a linearized graph (see Eq. 15) as shown in Fig. 9. Although the vertical scale on the graph is arbitrary, since the extinction coefficients for the new spectrum are not known a priori, the ω^2-axis is correctly calibrated. Despite more scatter in the data, the ω^2 intercept was close enough to that found by analysis using the R–T difference spectrum to prompt us to use the same value for the intercept as obtained from the R–T difference spectrum, and see if the resulting straight line fit the data. The lines so obtained are shown as the solid lines in Fig. 9; as can be seen, the fits are acceptable. The simplest interpretation of this result is that the unknown spectrum, extrapolated to zero power, and the R–T difference spectrum similarly extrapolated, are reporting the

same kinetic event, namely the R–T transition. Consequently, the slope should be the same (since the kinetics are the same), which in turn allows the scale of the y axis to be determined. Knowing the scale gives extinction coefficients for the spectrum by comparison of the slope obtained in this plot with that obtained in the R–T plot (e.g., Fig. 5). This procedure is what permits the scale of the y axis to be set in Fig. 3. Although the curves for pH 6.5 and pH 7.0 have the same shape (by assumption), the spectrum obtained at pH 6.5 has a maximum extinction coefficient about twice as large as that seen at pH 7.0.

DISCUSSION

Comparison with Other Experiments

Before examining the implications of the new data gathered by these experiments, we wish to consider the data measured here which is also accessible to other measurement techniques. The on-rate, k_R, has been previously determined by time-domain photolysis experiments (14, 17, 25). In our experiments this rate is determined by measuring the tangent of the absolute phase, which is dominated by the rate k_R[CO]. Our results are summarized in Table I. Because our samples were prepared in a glove box with imperfect hand seals, it is possible that some samples were not fully saturated with CO (the hemes were fully saturated, of course). This could account for the variation of CO binding rates for experiments repeated at the same pH. If we view the faster rate as indicative of the correct value, we find k_R is 5.7×10^6 M^{-1} s^{-1} for pH 7, and 4.9×10^6 M^{-1} s^{-1} for pH 6.5 DeYoung et al. found the corresponding rates for hemolysates in phosphate buffer to be 6×10^6 M^{-1} s^{-1} and 5×10^6 M^{-1} s^{-1} (25); Hofrichter et al. report a value for pH 7 in phsophate buffer of 6×10^6 M^{-1} s^{-1} (17); Sawicki and Gibson also report similar values (14). We thus conclude that our ligand binding rate constants are in good agreement with other studies.

From the ratio of the measured allosteric rates we obtain an equilibrium constant between R and T structures at threefold ligation. This constant, L_3, is also known by the measurement of equilibrium binding curves. Unfortunately, very few binding curves are available for CO, so we must compare our results with oxygen saturation curves. Imai and Yonetani have reported oxygen binding curves measured in phosphate buffer as a function of pH (26), and so we chose to use that data for purposes of comparison. The Adair constants determined in that study were used to regenerate saturation curves, which were then reduced to MWC parameters by least squares fitting. For pH 6.5 that data yields $L_3 = 0.49$ ($L = 5.4 \times 10^8$; $c = 0.002$), while for pH 7.0, $L_3 = 0.74$ ($L = 1.7 \times 10^7$; $c = 0.0035$). These values compare well with the direct measurement of our experiment, viz. 0.33–0.34. Since there are also known to be small differences between CO and O_2 as ligands (27), such agreement must be considered excellent.

The only other measurement of the rate of allosteric change with three ligands bound was the initial modulation study of Ferrone and Hopfield (18). As mentioned in the introduction, the discovery that 1–2% photolysis produced sufficient numbers of doubly deoxygenated molecules to interfere with the simple analysis of the data prompted us to reexamine the previous experiment. The most noticable effect of multiple excitation is that the linearized plots (see Eq. 15) exhibit curvature near the origin. This can be seen in Fig. 10 where we have replotted two of the data sets of Ferrone and Hopfield (18). The curves shown in Fig. 10 have been generated by using the allosteric rates from Table I. The only parameter varied in calculating these curves in the excitation rate, A_{Rj} in Eq. 4. The DC level of photolysis is found to be 14% for the 10% CO sample, and 1.4% for the nominally 100% CO sample. (It is also likely that full solution saturation was not maintained in the latter experiment.) As can be seen, the model reproduces the downward curvature of the data very well. We have also included a correction for the dimer population, calculated using standard values for the dimer-tetramer equilibrium constant (28, 29), which produces some additional curvature. We conclude that although the previous analysis was in error due to the failure of the assumption of small excitations, the present analysis rectifies this error, and accounts for the previous data as well.

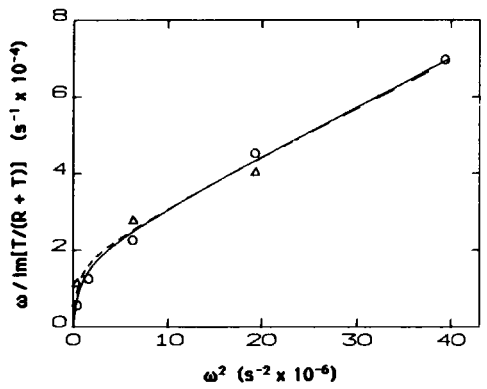

FIGURE 10 Analysis of the pH 7.0 data of Ferrone and Hopfield (18). Two data sets are shown: for the circles the solution was nominally saturated with CO; while for the triangles, only 10% of CO saturation of the solution was achieved. The curves use the pH 7.0 rates generated in this study, and differ from the original only in the analysis used on the data. We have varied only the excitation parameter A_{Rj} of Eq. 4 to obtain both curves shown; moreover, no extensive search was conducted for a best value of that parameter. (The curves show the results of $A_{Rj} = 8$ s^{-1}. This is quite similar to the values found in the present study; the differences lie in using extrapolation for the present data, and in the lower CO concentrations in the former study.) We deduce that the low CO saturation curve (solid curve and triangles) had a DC excitation of 14% of the sample hemes, while the high saturation sample (dashed curve and circles) had a DC excitation of 1.4% of the sample hemes. The decrease in excitation is expected since the dissociation rate was kept constant, but the reassociation rate varied with the CO concentration.

TABLE 1
KINETIC PARAMETERS FOR HbA

pH	k_{RT} ($10^3\ s^{-1}$)	k_{TR}* ($10^3\ s^{-1}$)	L_3‡	$K_R[CO]^3$ ($10^3\ s^{-1}$)
6.5	1.2	3.5	0.34	4.8 4.3
7.0	1.0	3.0	0.33	5.5 3.8

*Obtained with the assumption that $k_T[CO] = 100\ s^{-1}$.
‡Defined as k_{RT}/k_{TR}.
§Results are shown for two different experiments. Discrepancies are discussed in the text.

Implications of the Kinetic Data

The principal result of this work is the measurement of the rate of conformational change with three ligands bound at pH 6.5 and 7.0. Our results are summarized in Table I. The variation in allosteric rates with pH is definitely outside the instrumental uncertainties of the experiment. However, systematic sources of error can not so easily be determined. Particularly problematical for this experiment is the choice of accurate standard spectra; as described below, the spectra directly affect the rates measured. Unfortunately, we cannot exclude a pH dependence of the standard spectra that would produce the differences in k_{RT} observed. On the other hand, if such differences are present, they are not large, for we have seen no evidence in the ligand-binding spectra to suggest large pH dependent differences. In short, the accuracy is primarily limited by the spectroscopy of the standards, rather than the kinetic method used here.

When taken together with other information about the allosteric kinetics of hemoglobin, these rates provide insight into the regulation of the kinetics of structural change. The rate of transition between R and T for pH 7 for the fully deoxy species is found to lie between 4 and 5 × $10^4\ s^{-1}$ (16, 17); for a single ligand bound, the rate of transition drops to $1.4 \times 10^4\ s^{-1}$ (16). (Sawicki and Gibson found the rate to decrease with the binding of CO by a similar factor at higher pH [14].) When three CO molecules are bound, we find the R to T rate to be $1.0 \times 10^3\ s^{-1}$. This is in sharp contrast with the behavior of the equilibrium constant between R and T states, which changes dramatically over the same range. Without ligands, the allosteric equilibrium constant is of the order of 10^7 (10, 24), while with three ligands, it drops to 0.33. Thus it is the T to R rate which exhibits the strong variation as ligands are added. In the language of transition state theory this says that the structure of the transition state for the R to T transition is very similar to the reaction product, i.e., the T structure.

One explanation of this behavior derives from a conjecture put forth by Baldwin and Chothia (5) that the principal steric hindrance to the structural change is the movement of His β97 past Thr α41. Since these residues do not make significant contacts stabilizing either R or T structures (with the exception of a hydrogen bond in the R structure between Arg β40 and Thr α41) the reaction surface between R and T may be visualized as a composite of the potential wells which stabilize the R and the T structures, and a barrier which does not directly affect stability, as illustrated in Fig. 11 *a*. This composite nature means that events that act on the depth of one well affect

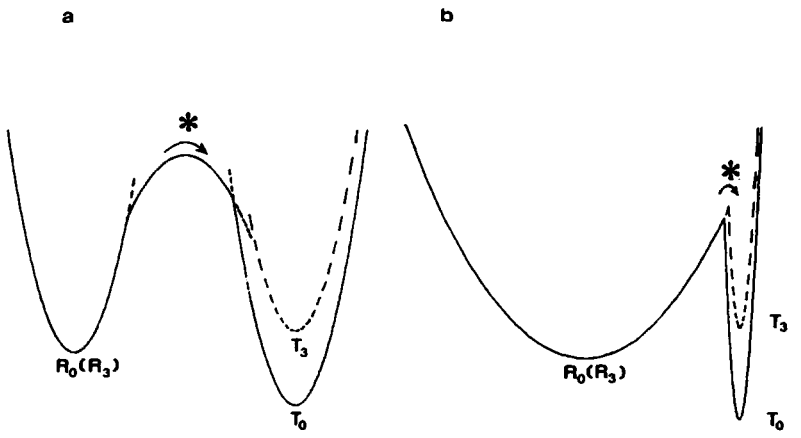

FIGURE 11 Possible schematic forms of the transition state (*) between quaternary structures. Both *a* and *b* show the total chemical potential of the molecule along the configurational coordinate used in going between alternative structures. (*a*) The R and T potential wells are separated by a region that is relatively unaffected by factors (e.g., ligand binding) that alter the stability of either well. The dashed line shows the T state potential curve with three ligands bound, when the R state potential wells for zero and three ligands are superimposed. The central potential barrier could correspond to the steric hindrance arising from the movement of His β97 past Thr α41, as proposed by Baldwin and Chothia (5). If the addition of ligands affects the stability of the T state, then the transition state will be T-like. As shown, changes in the depth of the T well affect where it joins the central barrier, rather than affecting the height of the transition state. (*b*) The transition state between structures is essentially represented by the crossing point between the potential wells. For the transition state to be T-like requires the T well to be substantially narrower than the R state well.

the point of intersection of that well and the barrier, rather than the point of intersection of the two wells. Transitions from the other well are therefore unaffected, since the barrier height in that direction is unchanged. In the case at hand, destabilization of the T state affects only the rate out of the T state, but not the rate out of the R state. If the conjecture by Baldwin and Chothia is correct, then, the observed T-like behavior of the transition state implies that the additions of ligands destabilizes the T state, rather than stabilizing the R state per se.

Given the scale of fluctuations in proteins, it may be that the steric hindrance posed by the movement of His β97 past Thr α41 is insignificant. In that case, we can consider the possibility that the reaction coordinate does not have a central barrier unconnected with stability, but rather that the reaction coordinate represents the crossing of the surfaces which describe the potential of the R or T structures as in Fig. 11 *b*. If so, the T character of the transition state could result from a number of interesting effects. For example, the formation of the bonds at the interface which stabilize the T state might be highly cooperative, so that the transition occurs only when most bonds are in place. Such an interpretation would be in keeping with the view that the R structure is primarily stabilized by hydrophobic forces rather than specific bonds, whereas the T state is just the opposite.

Nature of the New Spectral Feature

What is the source of the new spectral feature seen? Given its location it might be supposed that it arises from a perturbation of the spectrum of the liganded hemes. Such perturbations have been observed in certain systems. Liganded HbKansas (β102 Asn → Thr) shows a difference spectrum in the visible region upon the addition of the allosteric effector inositol hexaphosphate (IHP) (30). By a variety of measurements (10, 31, 32), HbKansas with IHP is found to be in the deoxy or T structure, suggesting that the spectral perturbation is a marker for structure. Hemoglobin Trout IV also is known to shift its structure with pH (33) and/or by addition of IHP, even when fully liganded (34). For CO liganded Trout hemoglobin, a Soret spectral feature is observed which is remarkably similar to that seen here (34). The difference spectrum for HbTrout IV is shown as the dashed line in Fig. 3. A smaller, but similar difference spectrum has also been observed for carboxyhemoglobin of the Carp with and without IHP (35). By other methods, Carp hemoglobin is also known to switch quaternary structures upon addition of IHP (36). In comparing the size of the extinction coefficients it is important to note that the allosteric equilibrium for liganded HbTrout IV + IHP has not been quantified. For example, if the liganded species with IHP had a 50% mixture of R and T states (i.e., $L_4 = 1$), the binding curves would be almost totally noncooperative, although the difference spectrum obtained would in fact be half of that seen if all molecules switched structure.

However, a more fundamental question must be raised. Is the new spectral feature truly independent of the familiar R–T difference spectrum, or is it possible that the static spectra do not represent the kinetic R–T difference spectra? First, let us examine the evidence present in this experiment. If the spectrum does arise from a perturbation of the liganded derivative as the structure changes, we expect the effective spectral shape in the out-of-phase data to change as we induce multiple excitations. This is because, for example, the doubly deligated species has two deoxy hemes and two liganded hemes, while the triligated species has one deoxy and three CO. As we increase the laser intensity, we would thus expect to see the contribution of the new spectrum decrease relative to the contribution of the R–T difference spectrum. (In contrast, if the new spectrum is merely an unanticipated portion of a single R–T difference spectrum, the relative contributions will not change as laser intensity is increased.) For the pH 6.5 data, we do observe a decrease in relative magnitudes as laser intensity increases; for the pH 7.0 data, the scatter does not permit us to draw a definite conclusion. Even for pH 6.5, this does not exclude the possibility that some part of the new spectral feature is responsive to the deoxy hemes; the data only demands that there be some part of the new spectrum which does not follow the same behavior as the deoxy hemes. Furthermore, while we cannot categorically exclude the possibility that this new spectral feature is responsive to a different kinetic process than the R–T change reported by the deoxy hemes, the above discussion also supports our assignment of the kinetic process.

In the literature there is some variation regarding the spectral signature expected from deoxy hemes when quaternary structure is changed. A spectral change in the deoxy hemes upon change of quaternary structure was first observed by Gibson in kinetic experiments (13), and has since been observed in a number of ways. In addition to the effect of IHP on NES des Arg Hb, the spectrum has been seen upon the aggregation of monomers to tetramers (37, 38), on the aggregation of dimers to tetramers (37, 27), on the addition of IHP to Hb Bethesda (37), and in other kinetic experiments (14, 15, 17). There do exist small differences among these spectra: the peak extinction coefficient ranges from as high as 21 $mM^{-1}\ cm^{-1}$ to as low as 15 $mM^{-1}\ cm^{-1}$, and the low wavelength zero crossing varies from as high as 413 nm to as low as 400 nm. However, all the spectra have a similar shape, with no evidence of the derivative type shape seen in the trout or carp difference spectra or in the new spectrum reported here. While the exact shape we deduce for the liganded allosteric difference spectrum may depend on the choice of standard deoxy allosteric spectrum, we do not believe that the general shape of the liganded R–T spectrum would be altered, or its existence brought into doubt.

It is easy to see that a spectral feature of this size could go unnoticed in previous kinetic studies (14, 15, 17). Those

experiments would, at most, be sensitive to the singly ligated species for kinetic reasons. However, a conformational difference spectrum for the singly ligated species will mix the standard deoxy R–T difference spectrum with the liganded R–T difference spectrum at the ratio of 3:1 (since three hemes are unligated). Such a spectrum is shown in Fig. 12; as can be seen, it remains quite similar to the standard R–T spectral difference (the dashed line), especially given the differences reported for that spectrum (see, e.g., ref. 37).

Implications for the Method

It is interesting to compare these results with those expected in a partial flash experiment. Assuming that only triligated species are produced, the population which rebinds from the R state is given by $R_3k_R/(k_R + k_{RT})$, while the population rebinding from T is given by $T_3k_T/(k_T + k_{TR})$. For the pH 7.0 data, this implies that only ~1% of the hemes would rebind slowly. In such partial flash experiments little biphasicity would be seen in the relaxation. If the reaction is followed at an isosbestic for ligand rebinding, as done by Sawicki and Gibson (14, 15), then it is possible to follow the growth and decay of the T_3 state in principle. However, a straightforward calculation readily shows that this signal is also small. The most effective strategy for this type of measurement would be to slow the ligand rebinding rate, e.g., by reducing the free CO concentration. With a solution 10% saturated with CO, the most T-state signal that would be observed, using the pH 7.0 values of this study, corresponds to about 15% of the total number of hemes excited. Typical partial flash experiments are done with 10–20% excitation (17, 24); this presents further problems. A 10% photolysis experiment will have 16% of its observed signal (1.6% of the total hemes) arise from double excitations. These doubly excited molecules are most likely to cross to the T_2 state at a different rate than the triligated species, and relax at a rate limited by $2k_T[CO]$. Thus an attempt to follow the kinetics at an isosbestic will need to resolve two quite similar processes for the typical 10% flash; lowering the photolysis level simplifies the analysis at the expense of signal level. In short, although the data gathered here can in principle be obtained with straightforward pulse techniques, such an approach would be faced with considerable experimental difficulties.

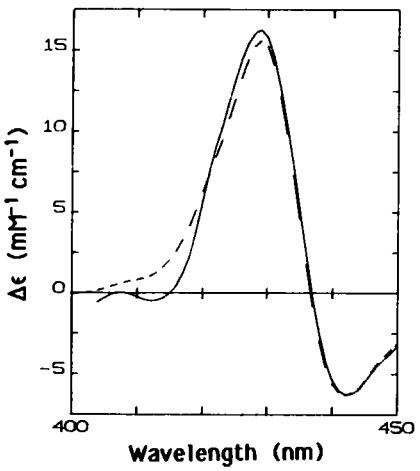

FIGURE 12 Hypothetical difference spectrum for the R–T conformational change with a single CO ligand. The dashed curve is the standard fully deoxy R–T difference spectrum of NES desArg Hb with and without IHP, taken from Perutz et al. (23). The small difference is due to the fact that such a molecular species has three deoxy hemes for every liganded heme undergoing the conformation change.

On the other hand, the method of modulated excitation is not well suited for experiments in the nanosecond regime. Resolution of such rapid kinetics requires a much higher modulation frequency than the kHz domain in which we are presently working. The difficulty arises not from the modulator (ours goes to a few MHz), but is the result of the need for a recyclable system. Since ligand binding cannot be arbitrarily accelerated, with a suitably high frequency we find $\omega \gg k_R$ and in this case the signal decreases as $1/\omega$. For example, with oxygen as a ligand (to give rapid recombination) at 1 MHz modulation, the overall signal will have fallen to 1.6×10^{-3} of its DC excitation value. Thus the extremely interesting tertiary events probed by nanosecond absorption (17) or resonance Raman (39) measurements appear beyond the scope of this technique, and can be viewed as instantaneous on the timescales accessible at present.

A principal limitation on the accuracy of the rates quoted here is due to uncertainty in the standard spectra. The day to day reproducibility of the data itself is at the level of 5%, whereas the standard R–T spectra (see above) can vary by as much as 30%. Uncertainty in the spectra directly (and proportionately) affects k_{RT}. The ω^2 intercept will still correctly give the sum $k_{RT} + k_{TR} + k_T$, but the uncertainty in k_{RT} will thus propagate to the other rates. We are presently investigating methods whereby an internal standard set of spectra can be generated for use in these experiments.

Regarding the precision of the experiments, practical limitations on the technique of modulated excitation make it unlikely that an additional order of magnitude improvement in signal to noise can be obtained without drastic changes in the apparatus. At present, running the spectra for a given frequency takes 10 to 15 min. Since the experiment is close to the shot noise limit, a decade improvement requires 100 times longer averaging. An important and immediate limitation that arises is that of phase tuning. If the noise level of the experiment is such that a 10 s averaging time is warranted, manual tuning to zero the out-of-phase component becomes a very slow procedure. The effects of mistuning are discussed in the Appendix. Work is underway in this laboratory to extend the method to other wavelength regions, and to minimize other noise sources such as laser fluctuations.

APPENDIX

Effect of Multiple Excitations

In this section we consider in an approximate way the effects of multiple excitations of a given tetramer, and thereby determine rough criteria for the small excitation limit. Originally, multiple excitations were expected to make a negligible contribution to the measured rates, especially with excitations at ~1% (18); however, numerical solution of the full modulated excitation equations using typical parameters have convinced us otherwise. The principal reason that multiple excitations are significant is that excitations from state R_3 to state R_2 are accompanied by relaxation to state T_2 (see Fig. 13 *a*). Given typical values for L_2 (~200), the rate from T_2 to R_2 is likely to be much slower than the R_2 to T_2 rate. With the values that are known for R–T rates at other degrees of ligation, the T_2 to R_2 rate is likely to be slower than the ligand binding rate $2k_T$. Thus the T_2 state assumes the character of a trap, from which relaxation will occur with the relatively slow rate $2k_T$. This affects the analysis in two ways. First, this process will represent an allosteric crossing, with different kinetics than expected between states R_3 and T_3. Second, the presence of the ligand rebinding signal from the multiply excited tetramer will alter the phase tuning, effectively adding a rotation of the vector V′ (Eq. 13) which is not considered in the simple analysis. We shall consider these in turn.

Some preliminaries are helpful. In the derivations below we shall be making use of the result that, for a simple relaxation process with rate k, excited at rate A, the oscillating population P is given by $P = AP_0/(k + i\omega)$, with P_0 being the equilibrium source or ground state population (18).

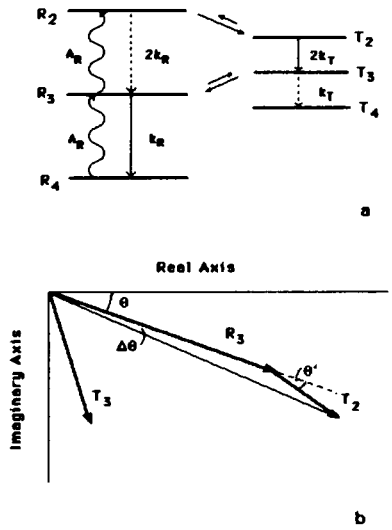

FIGURE 13 (*a*) Diagram of free energy levels involved in calculating the effect of multiple excitations. For clarity, states with 0 or 1 ligand bound are not shown. For the calculations in the appendix, we assume that the transition from R to T with two ligands bound is much faster than the reverse transition, or the ligand binding rate $2k_R$. This makes state T_2 an effective trap; depopulation of T_2 is presumed to be rate limited by $2k_T$. Excitations within the T states, and excitations to higher levels than shown are assumed negligible relative to the other processes shown. The small excitation limit assumes that states T_2 and R_2 are negligibly populated. (*b*) Population vector diagram illustrating phase relationships. The axis system describes phasing relative to the excitation, which defines the real axis. The diagram appears in the fourth quadrant because the excited population lags the excitation. In general, the phase angles and the lengths of the vectors depend on excitation frequency ω. In actuality, T_2 and T_3 are likely to be smaller than R_3 by a factor of ~100. Because of this, $\Delta\theta$ will be small. To determine the observed signal, each population vector must be scaled by its spectral weight, and the sum taken.

We shall use boldface letters to distinguish complex population vectors from the labels for states in this section. Also for convenience, we are suppressing the [CO] dependence of the ligand binding rates. Thus when we write k_T we really mean k_T[CO]. Finally, we shall denote the allosteric rates at threefold ligation without numerical subscripts as k_{RT} or k_{TR}.

First we consider the effects of crossings from R_2 to T_2. If we assume that the R_2 to T_2 transition is faster than the reverse transition, and faster than the excitation rate to R_2, then the populating of T_2 is rate limited by the excitation rate, A_R, and we may approximately write $\mathbf{T}_2 = A_R\,\mathbf{R}_3/(2k_T + i\omega)$. For comparison with the analysis in the small excitation limit we need $\mathrm{Im}[\mathbf{T}_2/(\mathbf{R}_3 + \mathbf{T}_3)] = \delta_1$. The correction ($\delta_1$) must be compared with the size of $\Gamma = \mathrm{Im}[\mathbf{T}_3/(\mathbf{R}_3 + \mathbf{T}_3)]$, given by Eq. 14, to which the correction will be added. After some algebra, and the assumption that $k_T \ll k_{RT}$ or k_{TR}, we find

$$\delta_1/\Gamma = (A_R/k_{RT})[\omega^2 + k_{TR}(k_{RT} + k_{TR})]/(\omega^2 + 4k_T^2).$$

Notice that this will go to zero as A_R goes to zero. Moreover, this correction will contribute to the pronounced curvature in the linearized data plots seen with excitation to the upper states (e.g., Fig. 10). This is because δ_1/Γ becomes essentially zero (namely, A_R/k_{RT}) at high frequencies, while at low frequencies δ_1/Γ can be substantial. If we take $k_T = 100\ s^{-1}$, with a typical value of $A_R = 8\ s^{-1}$, then at 50 Hz, $\delta_1/\Gamma = 0.70$; at 100 Hz $\delta_1/\Gamma = 0.23$, and at 1,000 Hz, $\delta_1/\Gamma = 0.01$. In this example, the fractional photolysis level (given by A_R/k_R) is a mere 0.13%. For lower values of k_T, the corrections are even greater; this is the case in Fig. 10.

The second correction arises from the phase tuning artifact. In the case of multiple excitations, there are two sources of ligand rebinding signals: single recombinations from R_3 and recombinations from doubly ligated species R_2. If we make the same assumption as above, i.e., that relaxation from R_2 to T_2 is rapid, then R_2 is a virtual state, and rebinding occurs from T_2 with rate $2k_T$. Our tuning procedure means that we shall tune along the vector sum, $\mathbf{R}_3 + \mathbf{T}_2$. The phase angle of $\mathbf{R}_3$ relative to its source (the DC population), is given by the angle θ. The phase angle of $\mathbf{T}_2$ relative to its source, $\mathbf{R}_3$, is θ'. (See Fig. 13) Our small excitation analysis depends upon tuning along the vector $\mathbf{R}_3$, with angle θ; instead we have tuned to an angle $\theta + \Delta\theta$. For simplicity we assume that the vector $\mathbf{R}_3$ is given by $\mathbf{R}_3 = A_R\mathbf{R}_4/(k_R + i\omega)$ and that as above $\mathbf{T}_2 = A_R\mathbf{R}_3/(2k_T + i\omega)$. Since $\tan\theta = -\omega/k_R$, the magnitude of $\mathbf{R}_3$ is $|\mathbf{R}_3/\mathbf{R}_4| = (A_R/k_R)\cos\theta$. Similarly $\tan\theta' = -\omega/2k_T$ and $|\mathbf{T}_2/\mathbf{R}_3| = (A_R/2k_T)\cos\theta'$. From these relationships and the law of sines,

$$\tan\Delta\theta = (A_R/2k_T)\sin 2\theta'/[2 - (A_R/k_T)\cos^2\theta'].$$

Since modulated excitation usually requires $A_R \ll 2k_T$, we can write $\tan\Delta\theta = (A_R/4k_T)\sin 2\theta' = -A_R\omega/(\omega^2 + 4k_T^2)$. In the presence of multiple excitations $\mathbf{T}_3$ will be measured in coordinates rotated by $\Delta\theta$. This means that in the rotated coordinates the imaginary part of $\mathbf{T}_3$ will decrease, and a portion of the real part will be projected in. The decrease of the imaginary part will be small because $\Delta\theta$ is small. Thus the major tuning correction will be given by $\delta_2 = -\mathrm{Re}[\mathbf{T}_3/(\mathbf{R}_3 + \mathbf{T}_3)]\sin\Delta\theta$. It is straightforward to show that $\mathrm{Re}[\mathbf{T}_3/(\mathbf{R}_3 + \mathbf{T}_3)] = k_{RT}(k_{TR} + k_{RT})/[(k_{TR} + k_{RT})^2 + \omega^2]$ where again we make the assumption that $k_T \ll k_{RT}$ or k_{TR}. Since we consider only small $\Delta\theta$, we set $\tan\Delta\theta \sim \sin\Delta\theta$. Hence

$$\delta_2/\Gamma = -A_R(k_{TR} + k_{RT})/(\omega^2 + 4k_T^2).$$

Again the correction goes to zero as A_R goes to zero. The magnitude of this second correction is also largest at low frequencies. For example, at 50 Hz, with the parameters used in the example above, $\delta_2/\Gamma = -0.23$; at 100 Hz, $\delta_2/\Gamma = -0.07$, and, as before, at large ω, δ_2/Γ goes to zero. Note that δ_1 has the opposite sign as δ_2, so that the two corrections cancel in part. For low frequencies, $\delta_2/\delta_1 = -L_3$, so that when the allosteric transition is uphill from R_3 to T_3 (i.e., $L_3 < 1$) the first correction term is more important than the second term. These effects are illustrated qualitatively in Fig. 4. The y-axis is essentially $\Gamma + \delta_1 + \delta_2$. The dependence on intensity arises from A_R. The fact that the slopes in Fig. 4

are positive reflects the dominance of δ_1 over δ_2. The frequency dependence of the corrections is also apparent.

The above calculations illustrate in an oversimplified way how multiple excitations can affect the measurement of the allosteric rates by modulated excitation. Our conclusion is that the small excitation limit depends both upon frequency and upon the rate constants of the system, so that while it is possible to tell a posteriori if the small excitation limit was reached, it is not so easy a priori. Even the sign of the net correction can change, depending on the rates of the allosteric transition. A more realistic approximation, albeit a more complicated one, would consider the case in which relaxation from R_2 to T_2 is not much faster than ligand rebinding from R_2. In the expressions given, k_T would have to be replaced by an effective rate, and in general the simple expressions will no longer hold. While it is clear that the corrections in both cases diminish at high frequencies, the criteria by which limits are decided are available only after the allosteric rates are known. Although it would be possible to gather only high frequency data, the absence of multiple excitation interference could only be shown in a self-consistent way. Unfortunately, the above calculations also illustrate that the complications of multiple excitations need not provide a means for determining the allosteric rates when two ligands are bound, for in the case considered here those rates have disappeared from the correction terms.

We thank Mr. Wolfgang Nadler for the design and construction of much of the electronics, Ms. Alison Hardcastle for help with the preparation of the hemoglobin, and Dr. Marilyn Bishop for assistance with the curve fitting routine. We also thank Drs. William Eaton and James Hofrichter for helpful discussions.

This work was supported by the National Institute of Arthritis, Diabetes, Digestive and Kidney Disease, of the National Institutes of Health, through grant AM 30239.

Received for publication 3 December 1984 and in final form 29 March 1985.

REFERENCES

1. Hammes, G. G. 1978. Control of the catalytic activity in enzymes. *Adv. Chem. Phys.* 39:177–212.
2. Gurd, F. R. N., and T. M. Rothgeb. 1979. Motion in proteins. *Adv. Prot. Chem.* 33:74–166.
3. Careri, G., P. Fasella, and E. Gratton. 1979. Enzyme dynamics: The statistical physics approach. *Annu. Rev. Biophys. Bioeng.* 8:69–97.
4. McCammon, J. A., and M. Karplus. 1980. Simulation of protein dynamics. *Annu. Rev. Phys. Chem.* 31:29–45.
5. Baldwin, J., and C. Chothia. 1979. Hemoglobin: the structural changes related to ligand binding and its allosteric mechanism. *J. Mol. Biol.* 129:175–220.
6. Szabo, A., and M. Karplus. 1972. A mathematical model for structure-function relations in hemoglobin. *J. Mol. Biol.* 72:163–197.
7. Johnson, M. L., and G. K. Ackers. 1982. Thermodynamic analysis of human hemoglobins in terms of the Perutz mechanism: extensions of the Szabo-Karplus Model to include subunit assembly. *Biochemistry.* 21:201–211.
8. Lee, A. and M. Karplus. 1983. Structure-specific model of hemoglobin cooperativity. *Proc. Natl. Acad. Sci. USA.* 80:7055–7059.
9. Johnson, M. L., B. W. Turner, and G. K. Ackers. 1984. A quantitative model for the cooperative mechanism of human hemoglobin. *Proc. Natl. Acad. Sci. USA.* 81:1093–1097.
10. Shulman, R. G., J. J. Hopfield, and S. Ogawa. 1975. Allosteric interpretation of hemoglobin properties. *Q. Rev. Biophys.* 8:325–420.
11. Gelin, B. R., and M. Karplus. 1977. The mechanism of tertiary structural change in hemoglobin. *Proc. Natl. Acad. Sci. USA.*. 74:801–805.
12. Gelin, B. R., A. Lee, and M. Karplus. 1983. Hemoglobin tertiary structural change on ligand binding. *J. Mol. Biol.* 171:489–559.
13. Gibson, Q. H. 1959. The photochemical formation of a quickly reacting form of hemoglobin. *Biochem. J.* 71:293–303.
14. Sawicki, C. A., and Q. H. Gibson. 1976. Quaternary conformational changes in human hemoglobin studied by laser photolysis of carboxyhemoglobin. *J. Biol. Chem.* 251:1533–1542.
15. Sawicki, C. A, and Q. H. Gibson. 1977. Quaternary conformational changes in human oxyhemoglobin studied by laser photolysis. *J. Biol. Chem.* 252:5783–5788.
16. Cho, K. C., and J. J. Hopfield. 1979. Spin equilibrium and quaternary structure change in hemoglobin A. *Biochemistry.* 18:5826–5833.
17. Hofrichter, J., J. H. Sommer, E. R. Henry, and W. A. Eaton. 1983. Nanosecond absorption spectroscopy of hemoglobin: elementary processes in kinetic cooperativity. *Proc. Natl. Acad. Sci. USA.* 80:2235–2239.
18. Ferrone, F. A., and J. J. Hopfield. 1976. Rate of quaternary structure change in hemoglobin measured by modulated excitation. *Proc. Natl. Acad. Sci. USA.* 73:4497–4501.
19. Hopfield, J. J., R. G. Shulman, and S. Ogawa. 1972. An allosteric model of hemoglobin: I. Kinetics. *J. Mol. Biol.* 61:425–443.
20. Williams, R. C., and K. Y. Tsay. 1973. A convenient chromatographic method for the preparation of human hemoglobin. *Anal. Biochem.* 54:137–145.
21. Perutz, M. F. 1968. Preparation of haemoglobin crystals. *J. Crystal Growth.* 2:54–56.
22. Ferrone, F. A., J. Hofrichter, and W. A. Eaton. 1985. Kinetics of sickle hemoglobin polymerization: I. Studies using temperature jump and photolysis techniques. *J. Mol. Biol.* In press.
23. Perutz, M. F., J. E. Ladner, S. R. Simon, and C. Ho. 1974. Influence of globin structure on the state of the heme. *Biochemistry.* 13:2163–2173.
24. Bevington, P. R. 1969. Data Reduction and Error Analysis for the Physical Sciences. McGraw Hill, New York. 232–242.
25. DeYoung, A., R. R. Pennelly, A. L. Tan-Wilson, and R. W. Noble. 1976. Kinetic studies on the binding affinity of human hemoglobin for the 4th carbon monoxide molecule, L_4. *J. Biol. Chem.* 251:6692–6698.
26. Imai, K., and T. Yonetani. 1975. pH dependence of the Adair constants of human hemoglobin. *J. Biol. Chem.* 250:2227–2231.
27. Antonini, E., and M. Brunori. 1971. Hemoglobin and Myoglobin in their Reactions with Ligands. Elsevier/North Holland, New York. 260–263.
28. Sawicki, C. A., and Q. H. Gibson. 1981. Tetramer-dimer dissociation of carboxyhemoglobin in the absence of dithionite. *Biophys. J.* 35:265–270.
29. Edelstein, S. J., M. J. Rehman, J. S. Olson, and Q. H. Gibson. 1970. Functional aspects of the subunit association-dissociation equilibria of hemoglobin. *J. Biol. Chem.* 245:4372–4381.
30. Perutz, M. F., J. V. Kilmartin, K. Nagai, A. Szabo, and S. R. Simon. 1976. Influence of globin structures on the state of the heme. *Biochemistry.* 15:378–387.
31. Castillo, C. L., S. Ogawa, and J. M. Salhany. 1978. Equilibrium and kinetic measurements of carbon monoxide binding to hemoglobin Kansas in the presence of inositol hexaphosphate. *Arch. Biochem. Biophys.* 185:504–510.
32. Shulman, R. G., S. Ogawa, and A. Mayer. 1982. The two-state model of hemoglobin. *In* Hemoglobin and Oxygen Binding. Chien Ho, editor. Elsevier/North Holland, New York. 205–210.
33. Wyman, J., S. J. Gill, H. T. Gaud, A. Colosimo, B. Giardina, H. A. Kuiper, and J. Brunori. 1978. Thermodynamics of ligand binding and allosteric transition in hemoglobins. Reaction of Hb Trout IV with CO. *J. Mol. Biol.* 124:161–175.
34. Giardina, B., F. Ascoli, and M. Brunori. 1975. Spectral changes and allosteric transition in trout hemoglobin. *Nature* (Lond.). 256:761–762.

35. Knowles, F. D., M. J. McDonald, and Q. H. Gibson. 1975. The origin of the Adams-Schuster difference spectrum of oxyhemoglobin. *Biochem. Biophys. Res. Commun.* 66:556–563.

36. Tan, A. N., and R. W. Noble. 1973. The effect of inositol hexaphosphate on the allosteric properties of Carp hemoglobin. *J. Biol. Chem.* 248:7412–7416.

37. Olson, J. S. 1976. Spectral differences between the α and β heme groups within human deoxyhemoglobin. *Proc. Natl. Acad. Sci. USA.* 73:1140–1144.

38. Sugita, Y. 1975. Differences in spectra of α and β chains of hemoglobin between isolated state and in tetramer. *J. Biol. Chem.* 250:1251–1256.

39. Scott, T. W., and J. M. Friedman. 1984. Tertiary-structure relaxation in hemoglobin: a transient Raman study. *J. Am. Chem. Soc.* 106:5677–5687.